Letter

ADVANCED PHOTONICS

Nonlinear thermal emission and visible thermometry

Zhihao Zhou,[a] Wei Liu,[b] Hengzhe Yan,[a] Xianfeng Chen,[b] and Wenjie Wan[a,b,*]

[a]Shanghai Jiao Tong University, University of Michigan–Shanghai Jiao Tong University Joint Institute, State Key Laboratory of Advanced Optical Communication Systems and Networks, Shanghai, China

[b]Shanghai Jiao Tong University, Department of Physics and Astronomy, Shanghai, China

Abstract. The control of thermal emission is of great importance for emerging applications in energy conversion and thermometric sensing. Usually, thermal emission at ambient temperature is limited to the mid- to far-infrared, according to the linear theory of Planck's law. We experimentally demonstrate a broadband nonlinear thermal emission in the visible-NIR spectrum within a quadradic nonlinear medium, which emits visible thermal radiation through a pump-driven nonlinear upconversion from its mid-IR components even at room temperature, unlike its linear counterpart which requires ultrahigh temperature. The broadband emission is enabled by the crucial random quasi-phase-matching condition in our nonlinear nanocrystal powders. Moreover, nonlinear thermal emission also permits visible thermometry using traditional optical cameras instead of thermal ones. This scheme paves the way to understand thermal radiation dynamics with nonlinearity in many fields, such as nonlinear heat transfer and nonlinear thermodynamics.

Keywords: thermal radiation; nonlinear optics; mid-infrared; up-conversion; sum-frequency generation; nanocrystal.

Received Apr. 20, 2022; revised manuscript received Jun. 2, 2022; accepted for publication Jun. 14, 2022; published online Jul. 6, 2022.

[DOI: 10.1117/1.AP.4.4.045001]

1 Introduction

Blackbody radiation is the most fundamental physical phenomenon in nature and occurs for almost all objects that have a temperature above absolute zero. The resulting thermal emission is in the form of radiative electromagnetic (EM) waves well-described by Planck's law,[1] in which the temperature term seems to be the only variable ruling the emission spectrum. At ambient temperature, the majority of emitted EM waves are limited to far and mid-infrared, significantly beyond the visible spectrum. It would request some dedicated detection schemes such as narrow-bandgap semiconductor infrared detectors requiring cryogenic temperatures[2,3] and microbolometer thermal detectors but with a lower detection efficiency.[4] In this aspect, how to control such thermal emissions, e.g., spectra, becomes an emerging area with its potentially high-impact applications in thermal imaging,[5–8] spectroscopy,[9–12] energy conversion,[13] heat transfer,[14–16] radiative cooling,[17–19] and thermal management.[20–22] Thanks to the development of nanofabrication, many studies have focused on nano/microstructured thermal emitters,[23–26] to spectrally tune or confine the emission spectra in a designed manner. However, these thermal emissions still obey Planck's law, where the nano/microstructures only function as a linear filter in the spectral domain.

Although most of these prior works are limited to the linear regime, some theoretical proposals have recently emphasized the nonlinear dynamics of thermal radiation by introducing extra optical nonlinearity, e.g., the Kerr effect. In this manner, the original Planck distribution in the spectrum can be greatly altered for various novel applications like near-field heat transfer,[27] thermal refrigeration,[28] and thermal upconversion.[29] However, the low conversion efficiency is the main issue halting the experimental realization of these theoretical proposals. Although many of these works have studied resonant enhancement techniques such as plasmonic antenna[30] and optical microresonator,[31] they have ignored the phase-matching condition, which is the critical factor to determine the nonlinear conversion efficiency. Such phase-mismatching is due to the massive wavelength differences between thermal photons in far/mid-infrared and their converted ones like visible photons, hence greatly trimming the conversion efficiency.

*Address all correspondence to Wenjie Wan, wenjie.wan@sjtu.edu.cn

In this work, we experimentally demonstrate broadband nonlinear thermal emission in the visible-NIR spectrum from a medium of second-order optical nonlinearity. Under the illumination of an external pump laser, such a nonlinear medium emits visible thermal radiation through a sum-frequency upconversion from its mid-IR components, even near room temperature, unlike its linear counterpart requiring ultrahigh temperature. Broadband emission is enabled by the random quasi-phase-matching condition in our nonlinear nanocrystal powders, which critically determines the nonlinear upconversion process. Temperature-dependent emission also reveals its root from classical linear thermal radiation. Moreover, polarization properties of emission are also investigated. Such nonlinear thermal emission also enables a practical application in visible thermometry, which can be readily measured by commonly visible detectors such as cameras, without the need for expensive and highly demanding mid-IR detectors. This scheme opens new avenues for many fields in nonlinear heat transfer and nonlinear thermodynamics.

2 Principles and Methods

The general working principle of a nonlinear thermal emitter is depicted in Fig. 1, where the thermal emitter with second-order nonlinearity[2] at a temperature T is illuminated with an intense pumping laser. As a result, the traditional thermal emission spectra in the mid- to far-infrared, distributed according to Planck's law, can be readily upconverted into the visible and near-infrared regime through sum-frequency generation (SFG). This process extends the emission spectrum into the visible band. Unlike prior works relying on self-nonlinear wave mixing of thermal photons,[29,30] here, the upconverted photons are determined by both the temperature and external pump laser, giving us a unique tool to regulate thermal emission besides traditional temperature control. Here, the nonlinear upconversion process inside the thermal emitter with second-order nonlinearity can be described as[32,33]

$$E_{\text{vis}} = \frac{2\omega_{\text{vis}}}{n_{\text{vis}}c} E_{\text{pump}} E_{\text{IR}} \sum_{m=1}^{n} d_{\text{eff},m} \frac{e^{-i\Delta k X_m} - 1}{\Delta k} e^{-i\Delta k \sum_{j=1}^{m-1} X_j}, \quad (1)$$

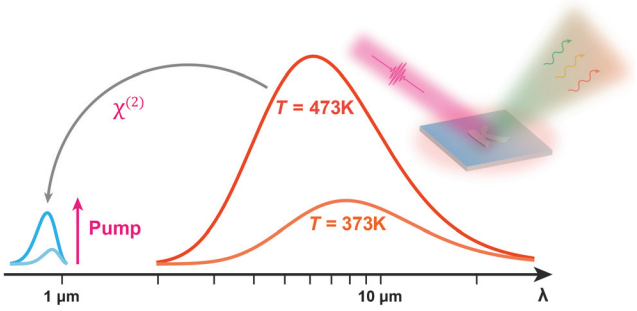

Fig. 1 Nonlinear thermal emission through nonlinear upconversion. A 1064-nm pump laser is used to convert mid-IR thermal radiation into visible wavelengths through the sum-frequency generation in a medium containing a quadratic nonlinearity. With the presence of optical pumping, a thermal object can simultaneously emit thermal radiation at both visible-NIR and mid-IR spectral bands.

where E_i, ω_i, n_i $(i = \text{vis}, \text{pump}, \text{IR})$ are electric field amplitudes, angular optical frequencies, and refractive indices of the three interacting waves, i.e., upconverted visible light, pump laser, and thermal infrared, respectively; $d_{\text{eff},m} = 1/2\chi_m^{(2)}(\omega_{\text{vis}}: \omega_{\text{pump}} + \omega_{\text{IR}})$ is the effective nonlinear coefficient of the mth domain/scatter, while X_m is the corresponding interaction length; Δk is the wavevector mismatch factor; and the last term $\exp(-i\Delta k \sum_{j=1}^{m-1} X_j)$ is the accumulated phase from multiple domains, holding the key for the quasi-phase-matching condition.

Traditionally, in a plain and homogonous crystal, accumulated phases from multiple domains may not be perfectly aligned up to the in-phase condition, leading to a low nonlinear efficiency, known as phase mismatch.[33] Especially, in the current setup, i.e., the SFG process involved with thermal photons in the far-infrared and upconverted visible photons, the associated phase-mismatching Δk is considerable. This explains why the current work was hardly observed previously. To solve the problem, many approaches have been proposed, e.g., using periodically poled lithium niobate[34] but with a narrow working spectral bandwidth. For broadband emissions like thermal radiation, such a phase-matching scheme is limited. Alternatively, the photonic system made up of disordered nanocrystals enables a novel phase-matching mechanism, i.e., random quasi-phase-matching (RQPM), where random sizes, positions, and orientations have averaging effects, smearing out the phase discrepancy for different interacting wavelengths. It has been shown that such an RQPM technique can greatly enhance second-order processes.[32,35–37] Moreover, it is proved to possess extremely loose frequency selectivity and ultrawide spectral tunability, making such a system an ideal platform for realizing nonlinear thermal radiation.

In our experiment shown in Fig. 2, we prepare a disordered and nonlinear sample by grinding $LiNbO_3$ material into miniaturized nanocrystals [Fig. 2(b)], which are then deposited onto an ITO substrate through electrophoresis deposition[38] with a film thickness of ~50 μm. Temperature control is realized by a ceramic heater combined with a PID controller [Fig. 2(a)]. Experimentally, the heated powder sample is optically pumped with a 1064-nm femtosecond laser (Fianium FP 1064/532-fs), and its thermal emission spectrum with a temperature up to 523 K is then collected by a spectrometer (Princeton Instruments SP2300i + Andor Newton DU970P-BV). Meanwhile, a comparison spectrum emitted from a bulk $LiNbO_3$ crystal with a similar thickness is also measured. In sharp contrast, while no visible emission is obtained in the bulk crystal's spectrum, the disordered sample's spectrum depicts an emission tail starting from 725 nm and grows to the longer wavelength range (up to 900 nm limited by the spectrometer), which is contributed from the sum-frequency of the pump and the thermal emission under the RQPM condition.

To further confirm the origin of the observed spectrum from disordered nanocrystals, we follow a theoretical treatment dealing with the RQPM scheme,[32,36] where the random sample can be modeled as a one-dimensional layered structure stacked along the propagation direction with varying thicknesses and orientations.[36] Specifically, the key component that enables RQPM is the accumulated phase term $\exp(-i\Delta k \sum_{j=1}^{m-1} X_j)$ in Eq. (1). After the signal propagates through several domains, a random relative phase is expected for the three interacting waves. In this case, the spectral intensity of nonlinear thermal

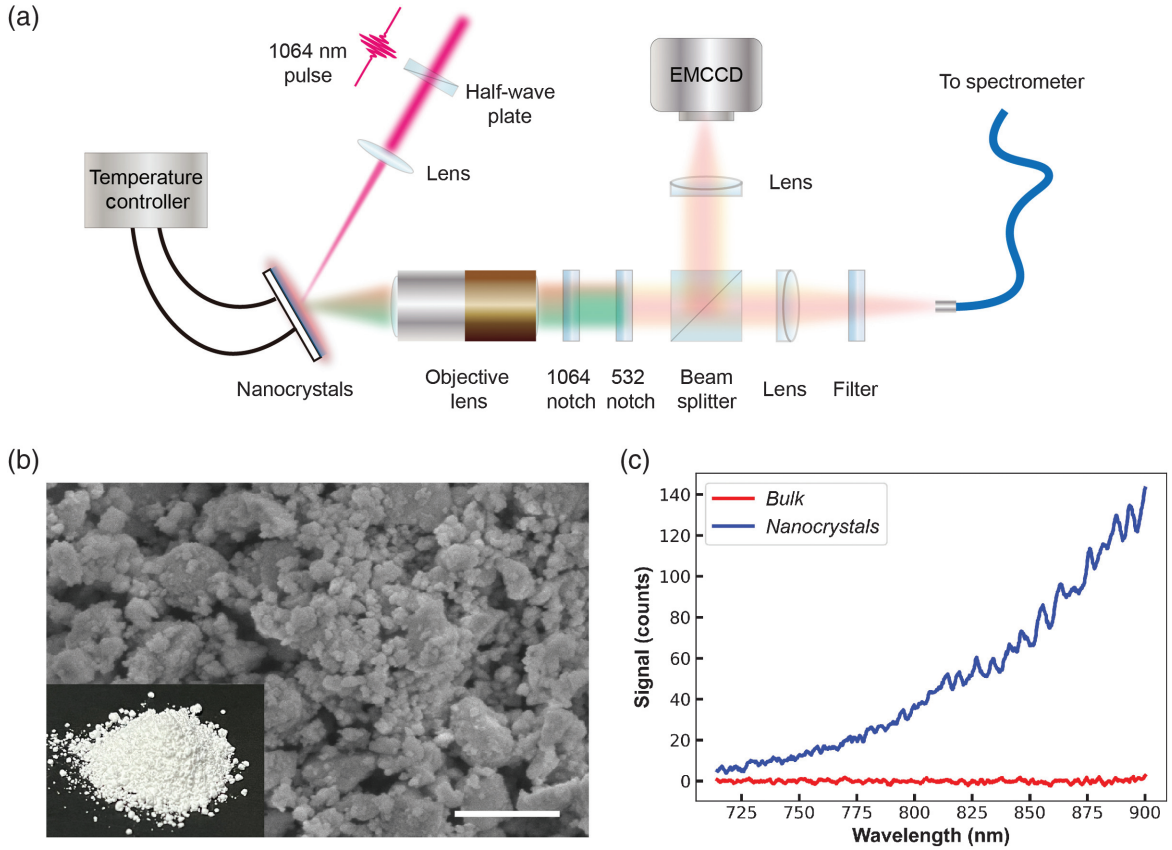

Fig. 2 Nonlinear thermal emission enabled by random quasi-phase-matching. (a) Experimental schematics: signals emitted from the thermal target are filtered with notch filters to reject fundamental, second-harmonic of the pump beam, and then split into two paths, which are further collected by an imaging system and spectrometer, respectively. (b) SEM image of $LiNbO_3$ nanocrystals ground from bulk $LiNbO_3$, which ensures the random quasi-phase-matching condition (scalebar: 1 μm). The inset shows the image of $LiNbO_3$ powder in real color. (c) The spectral signal is collected from a bulk $LiNbO_3$ crystal and random nanocrystals, where both targets are heated to 533 K and pumped with a 500-mW femtosecond beam at 1064 nm. While the disordered sample depicts a growing spectral signal, no visible signal is observed from the bulk one's spectrum.

radiation in the visible range can be derived by averaging over the ensemble of N domains as[32]

$$I_{\mathrm{vis}}(\lambda_{\mathrm{vis}},\lambda_{\mathrm{IR}},T) = \frac{8\pi^2}{\varepsilon_0 c\lambda_{\mathrm{vis}}^2}\frac{N\langle|d_{\mathrm{eff}}|^2\rangle}{n_{\mathrm{vis}}n_{\mathrm{pump}}n_{\mathrm{IR}}}\langle X^2\,\mathrm{sinc}^2(\Delta kX/2)\rangle I_{\mathrm{pump}}I_{\mathrm{IR}}(\lambda_{\mathrm{IR}},T), \tag{2}$$

where $\langle|d_{\mathrm{eff}}|^2\rangle = \int_\theta\int_\phi|d_{\mathrm{eff}}(\theta,\phi)|^2p(\theta,\phi)\mathrm{d}\theta\,\mathrm{d}\phi$ is the averaged effective nonlinear coefficient contributed from all possible geometric orientations $p(\theta,\phi)$, and $\langle X^2\,\mathrm{sinc}^2(\Delta kX/2)\rangle = \int_0^\infty X^2\,\mathrm{sinc}^2(\Delta kX/2)p(X)\mathrm{d}X$ is the averaged phase mismatch factor from varying interaction lengths across different nanocrystal domains; $I_{\mathrm{IR}}(\lambda_{\mathrm{IR}},T) = \int_S\int_\Omega\varepsilon(\lambda_{\mathrm{IR}})B(\lambda_{\mathrm{IR}},T)\mathrm{d}S\,\mathrm{d}\Omega$ is the thermal radiation spectral density, where $\varepsilon(\lambda_{\mathrm{IR}})$ is the sample's emissivity, and $B(\lambda_{\mathrm{IR}},T)$ is the spectral intensity of a perfect blackbody. I_{pump} is the pump intensity; λ_{vis} can be determined uniquely from λ_{IR} through energy conservation, i.e., $1/\lambda_{\mathrm{vis}} = 1/\lambda_{\mathrm{pump}} + 1/\lambda_{\mathrm{IR}}$. The two average terms can be treated as constants after averaging over specific probability density distributions.

3 Results

The important consequence of Eq. (2) is that the spectral intensity of nonlinear thermal radiation in the visible range directly resembles that of the sample's mid-IR thermal radiation, but it is further modulated with the inverse square of the visible wavelength as

$$I_{\mathrm{vis}}(\lambda_{\mathrm{vis}},\lambda_{\mathrm{IR}},T) \propto \frac{1}{\lambda_{\mathrm{vis}}^2}I_{\mathrm{IR}}(\lambda_{\mathrm{IR}},T) = \frac{1}{\lambda_{\mathrm{vis}}^2}\varepsilon(\lambda_{\mathrm{IR}})B(\lambda_{\mathrm{IR}},T) = \frac{1}{\lambda_{\mathrm{vis}}^2}\alpha(\lambda_{\mathrm{IR}})B(\lambda_{\mathrm{IR}},T), \tag{3}$$

where $\alpha(\lambda_{\mathrm{IR}})$ is the sample's absorptivity. According to Kirchhoff's law, the sample's emissivity must equal its absorptivity in thermodynamic equilibrium, which offers us a

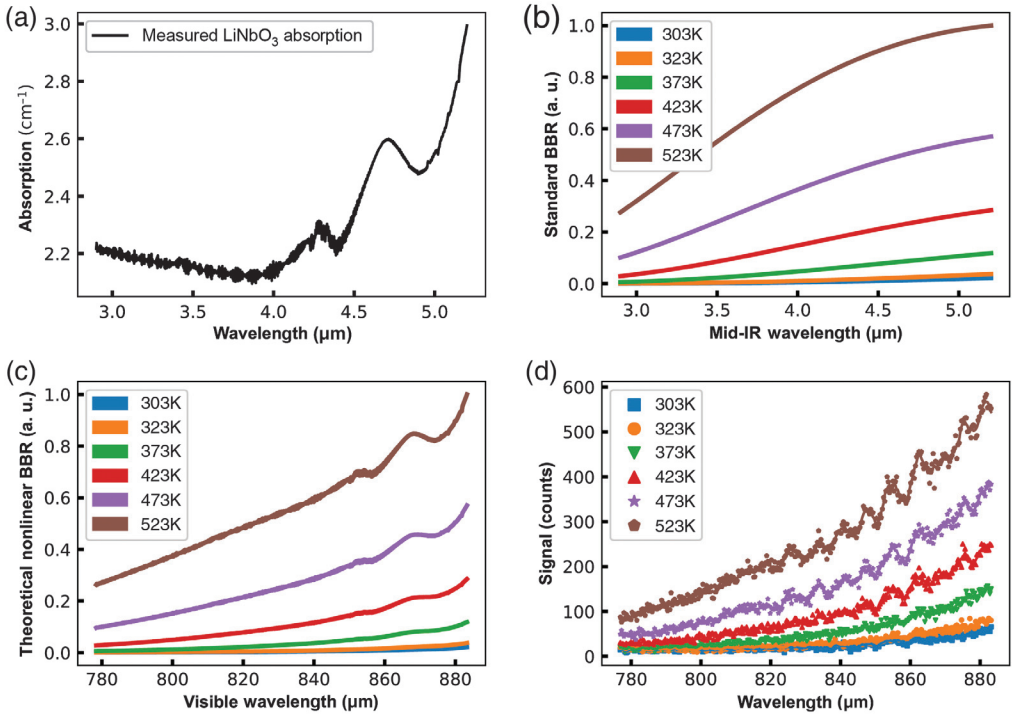

Fig. 3 The spectra of nonlinear thermal emission. (a) The absorption coefficient of $LiNbO_3$ at wavelength from 2.9 to 5.2 μm measured by FTIR spectroscopy. (b) Ideal blackbody radiation under different temperatures predicted by Planck's law. (c) Theoretically calculated nonlinear thermal emission of $LiNbO_3$ according to Kirchhoff's law. As the temperature grows from 303 to 523 K, the intensity of nonlinear thermal radiation keeps growing because of a substantial increase of blackbody radiation in the corresponding mid-IR range. (d) Experimentally measured spectra of nonlinear thermal emission with various temperatures.

convenient tool to model the emissivity through absorptivity measurements. Experimentally, the absorption coefficient of $LiNbO_3$ material [Fig. 3(a)] is measured by Fourier-transform infrared spectroscopy (FTIR) in the wavelength range of 2.9 to 5.2 μm, which corresponds to the observed nonlinear thermal emission around 780 to 883 nm. The absorption coefficient grows with increasing wavelength and finally becomes almost opaque around 6 μm. Combined with the theoretical curves of $B(\lambda, T)$ using Planck's law [Fig. 3(b)], we can further deduce the theoretical model of nonlinear thermal emission I_{vis} according to Eq. (3) under various temperatures, as shown in Fig. 3(c).

The key finding of this work is shown as experimentally measured visible emission spectra in Fig. 3(d). With temperatures varying from 303 to 523 K, the overall intensity envelopes of nonlinear thermal radiation grow substantially, corresponding to the naturally rising thermal spectra in the mid-IR range [Fig. 3(b)] under a constant pump (~500 mW). For each spectrum at a specific temperature, it keeps monotonously increasing to the longer wavelength side, and this trend is also confirmed by the theoretical results in Fig. 3(c). However, these rising trends are not exactly duplicating their counterpart in the mid-IR [Fig. 3(b)], mainly due to modification from the absorptivity [Fig. 3(a)] and term $1/\lambda_{\text{vis}}^2$ in Eq. (3). Moreover, the overall irradiance increases with temperature due to the broadband response of nonlinear conversion enabled by RQPM. As a result, the specific target temperature can be linked to the irradiant spectrum directly. Previously, thermal photon noise has also been observed in the nonlinear upconversion detector,[34] but the spectra of upconverted thermal radiation and its trend concerning temperature varying are different from the current work. This might be attributed to the quasi-phase-matching mechanism adopted in the upconversion detector to improve nonlinear efficiency, which inevitably leads to narrow-band conversion, while our current RQPM scheme provides flat and broadband nonlinear conversion efficiency over a wide mid-IR wavelength range (see Supplementary Material). Note that we also observe some slight oscillations in the experimentally observed spectra, which may be contributed by the interference in our free-space optics components.

More physical insights into nonlinear thermal emission can be found in their pump dependence and polarization properties in Fig. 4. Equation (2) reveals that nonlinear thermal emission linearly depends on the pump power, i.e., $I_{\text{vis}}(\lambda_{\text{vis}}) \propto I_{\text{pump}}$, regardless of wavelength or temperature. Experimentally, multiple spectra [Fig. 4(a)] at a temperature of 473 K are collected by varying the pump power from 400 to 1200 mW. The nonlinear thermal emission grows not only in peak value but also in the spectral width when the pump power increases. By summing over the spectra, the total irradiance of nonlinear blackbody radiation can be obtained for each pump power, resulting in a linear correlation curve, as shown in the inset of Fig. 4(a). This experimental evidence originates from the nature of the second-order nonlinear process, as indicated in Eq. (2).

Another feature of RQPM is that this second-order SFG is insensitive to the incident beam's polarization states, which originates from random orientations and sizes of the nanocrystals.

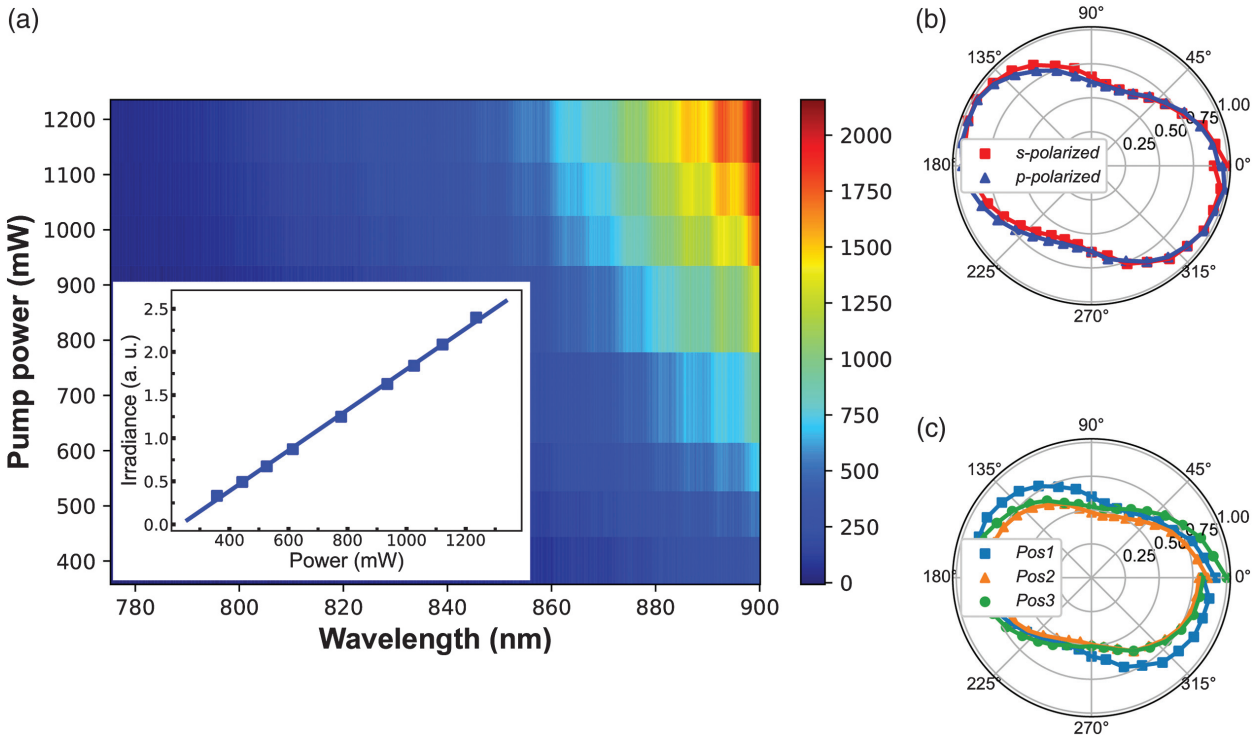

Fig. 4 Pump-power dependence and polarization properties of nonlinear thermal emission. (a) Experimental results of nonlinear thermal emission show a clear growing trend of irradiance when the pump power increases. Inset shows that the overall irradiance is linearly dependent on the pump power by summing over the entire spectral range. (b) Measured far-field polarization patterns of the emission under two orthogonal pump polarizations, indicating insensitivity of the signal on pump polarizations. (c) Far-field polarization patterns collected from three randomly picked locations. The overall polarization state of nonlinear thermal emission remains unchanged, but the intensity varies because of local anisotropy.

In contrast, for the phase-matched case, the nonlinear signal is highly dependent on the input beam, while even a slight change of polarization state can cause a significant modification to the overall conversion efficiency. In the current work, the observed polarization states in the far-field angular spectrum remain unchanged, even if the pump beams' polarizations are orthogonal to each other [Fig. 4(b)], which suggests that this thermal emission is dominated by local anisotropy in the sample. Such anisotropy may be introduced during the electrodeposition process with a high voltage (~150 V). Similar results were also reported in Ref. 37, where it was found that signal intensity increased as the aggregated size of the nanocrystal grew due to longer scattering paths. We further examine far-field polarizations of nonlinear thermal emission at three random locations. The results in Fig. 4(c) do reveal some slight variations, which might be contributed by different scattering paths, but the overall polarization patterns remain similar among the spectra at the three positions.

Lastly, in Fig. 5, the nonlinear thermal emission enables a practical application in thermometry, which can be readily measured by commonly visible cameras, without the need for expensive and highly demanding mid-IR detectors. Here, a metal mask engraved with the letter "*K*" is filled with $LiNbO_3$ nanocrystals to ensure the random quasi-phase-matching condition. The mask is also placed on the same heater, and the whole imaging target is illuminated by the pump beam. Images under different temperatures measured by a silicon-based EMCCD are shown in Fig. 5(a). Compared with traditional thermal imaging, these results are of much higher resolution determined by the diffraction limit. Temperature-dependent distributions are observed in the image profiles with an optical resolution, e.g., hot spots are concentrated at the intersection region. On the other hand, just like traditional thermometry with mid-IR light, we can also infer the local temperature according to its spectral irradiance from these visible thermal images, as the images become brighter when the temperature increases [Fig. 5(a)]. For a local spot, we logarithmically integrate the irradiance over part of the spectrum and relate it to temperature. As shown in Fig. 5(b), an inversely proportional relationship is observed over the test temperature range (130°C to 200°C) and fits well with the theoretical form ($\sum \ln^{\mathrm{Signal}(\lambda_{\mathrm{vis}},T)} \propto T^{-1}$) derived from Eq. (3) by incorporating Planck's law (see Supplementary Material). This thermometry technique not only achieves thermal imaging with an improved resolution, but also paves the way for low-cost thermometry using standard equipment in the visible spectrum.

4 Discussion and Conclusion

We experimentally demonstrate a broadband nonlinear thermal emission in quadradic nanocrystal powders. The random quasi-phase-matching scheme ensures broadband nonlinear upconversion from the mid-IR radiation into the visible-NIR spectrum.

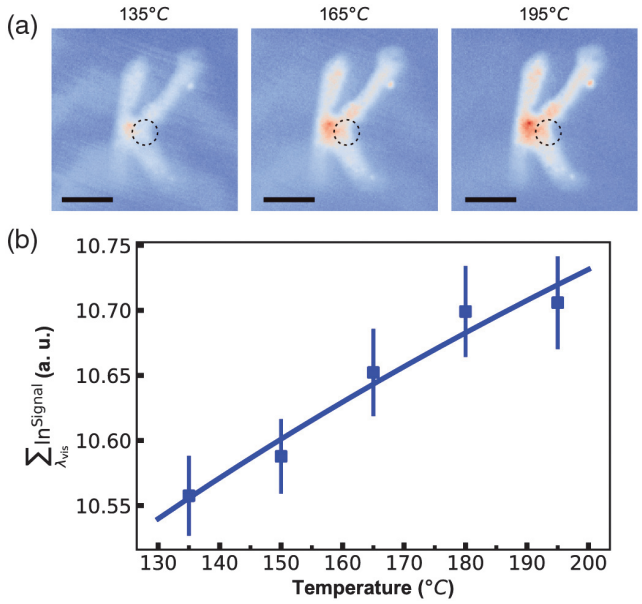

Fig. 5 Demonstration of visible thermometry. (a) Visible images of a letter "*K*" made of $LiNbO_3$ nanocrystals under different temperatures (scalebar: 100 μm). Overall, the captured visible thermal image becomes brighter as the target's temperature increases. Nonuniform signals inside the target suggest local hot spots. A dashed circle indicates the region used to calibrate the irradiance-temperature relationship. (b) Calibration curve of the relationship between signal and target temperature derived from Eq. (3). In this manner, we can accurately determine the temperature of the interested region via its emission intensity. Here, the thermometry resolution is only dependent on the optical resolution of the microscopic system.

Such nonlinear thermal emission also enables a practical application in thermometry, which can be readily measured by common visible detectors, e.g., cameras, without the need for expensive and highly demanding mid-IR detectors. There are a few potential applications, e.g., the demonstrated visible thermometry theoretically has a much better resolution defined by the diffraction limit,[39] while commercial mid-IR focal plane arrays have low-pixel density and require cryogenic operation. In comparison, this nonlinear thermal emission in the visible-NIR spectrum can be easily detected by traditional silicon-based CCDs with high resolution and sensitivity. Second, such nonlinear thermal emission may enable thermography through opaque media, e.g., water, which is highly absorptive in the mid-IR, but transparent with visible light. By converting thermal radiation into visible wavelengths, the temperature of the water-immersed target can be obtained remotely. We believe that nonlinear thermal emission will open new avenues for many fields in nonlinear heat transfer and nonlinear thermodynamics.

Acknowledgments

This work was supported by the National Natural Science Foundation of China (Nos. 92050113 and 11674228), the National Key Research and Development Program of China (Nos. 2016YFA0302500 and 2017YFA0303700), and the Shanghai MEC Scientific Innovation Program (No. E00075).

References

1. M. Planck, *The Theory of Heat Radiation*, Blakiston's Son & Co., Philadelphia (1914).
2. A. Rogalski, "HgCdTe infrared detector material: history, status and outlook," *Rep. Prog. Phys.* **68**, 2267 (2005).
3. C. L. Tan and H. Mohseni, "Emerging technologies for high performance infrared detectors," *Nanophotonics* **7**, 169–197 (2018).
4. R. K. Bhan et al., "Uncooled infrared microbolometer arrays and their characterisation techniques," *Def. Sci. J.* **59**, 580 (2009).
5. J. S. Dam, P. Tidemand-Lichtenberg, and C. Pedersen, "Room-temperature mid-infrared single-photon spectral imaging," *Nat. Photon.* **6**, 788–793 (2012).
6. L. M. Kehlet et al., "Infrared upconversion hyperspectral imaging," *Opt. Lett.* **40**(6), 938–941 (2015).
7. A. Barh, C. Pedersen, and P. Tidemand-Lichtenberg, "Ultra-broadband mid-wave-IR upconversion detection," *Opt. Lett.* **42**, 1504–1507 (2017).
8. R. Camacho-Morales et al., "Infrared upconversion imaging in nonlinear metasurfaces," *Adv. Photon.* **3**, 036002 (2021).
9. A. Xomalis et al., "Detecting mid-infrared light by molecular frequency upconversion in dual-wavelength nanoantennas," *Science* **374**(6572), 1268–1271 (2021).
10. W. Chen et al., "Continuous-wave frequency upconversion with a molecular optomechanical nanocavity," *Science* **374**(6572), 1264–1267 (2021).
11. L. Høgstedt et al., "Low-noise mid-IR upconversion detector for improved IR-degenerate four-wave mixing gas sensing," *Opt. Lett.* **39**(18), 5321–5324 (2014).
12. K. E. Jahromi et al., "Mid-infrared supercontinuum-based upconversion detection for trace gas sensing," *Opt. Express* **27**(17), 24469–24480 (2019).
13. A. Lenert et al., "A nanophotonic solar thermophotovoltaic device," *Nat. Nanotechnol.* **9**, 126–130 (2014).
14. E. Rousseau et al., "Radiative heat transfer at the nanoscale," *Nat. Photon.* **3**, 514–517 (2009).
15. K. Kim et al., "Radiative heat transfer in the extreme near field," *Nature* **528**, 387–391 (2015).
16. J. C. Cuevas and F. J. García-Vidal, "Radiative heat transfer," *ACS Photonics* **5**(10), 3896–3915 (2018).
17. A. P. Raman et al., "Passive radiative cooling below ambient air temperature under direct sunlight," *Nature* **515**, 540–544 (2014).
18. Y. Zhai et al., "Scalable-manufactured randomized glass-polymer hybrid metamaterial for daytime radiative cooling," *Science* **355**(6329), 1062–1066 (2017).
19. T. Li et al., "A radiative cooling structural material," *Science* **364**(6442), 760–763 (2019).
20. L. Zhu et al., "Radiative cooling of solar cells," *Optica* **1**(1), 32–38 (2014).
21. L. Zhu, A. P. Raman, and S. Fan, "Radiative cooling of solar absorbers using a visibly transparent photonic crystal thermal blackbody," *Proc. Natl. Acad. Sci. U. S. A.* **112**(40), 12282–12287 (2015).
22. X. Sun et al., "Optics-based approach to thermal management of photovoltaics: selective-spectral and radiative cooling," *IEEE J. Photovoltaics* **7**, 566–674 (2017).
23. N. Liu et al., "Infrared perfect absorber and its application as plasmonic sensor," *Nano Lett.* **10**, 2342–2348 (2010).
24. X. Liu et al., "Taming the blackbody with infrared metamaterials as selective thermal emitters," *Phys. Rev. Lett.* **107**, 045901 (2011).
25. T. Asano et al., "Near-infrared–to–visible highly selective thermal emitters based on an intrinsic semiconductor," *Sci. Adv.* **2**(12), 1600499 (2016).
26. X. Zhang et al., "Controlling thermal emission by parity-symmetric Fano resonance of optical absorbers in metasurfaces," *ACS Photonics* **6**, 2671–2676 (2019).
27. C. Khandekar et al., "Giant frequency-selective near-field energy transfer in active–passive structures," *Phys. Rev. B* **94**, 115402 (2016).

28. C. Khandekar, R. Messina, and A. W. Rodriguez, "Near-field refrigeration and tunable heat exchange through four-wave mixing," *AIP Adv.* **8**, 055029 (2018).
29. C. Khandekar and A. W. Rodriguez, "Near-field thermal upconversion and energy transfer through a Kerr medium," *Opt. Express* **25**, 23164–23180 (2017).
30. C. Khandekar et al., "Quantum nonlinear mixing of thermal photons to surpass the blackbody limit," *Opt. Express* **28**, 2045–2059 (2020).
31. C. Khandekar, Z. Lin, and A. W. Rodriguez, "Thermal radiation from optically driven Kerr ($\chi^{(3)}$) photonic cavities," *Appl. Phys. Lett.* **106**, 151109 (2015).
32. M. Baudrier-Raybaut et al., "Random quasi-phase-matching in bulk polycrystalline isotropic nonlinear materials," *Nature* **432**, 374–376 (2004).
33. R. W. Boyd, *Nonlinear Optics*, Academic Press (2020).
34. A. Barh, P. Tidemand-Lichtenberg, and C. Pedersen, "Thermal noise in mid-infrared broadband upconversion detectors," *Opt. Express* **26**, 3249–3259 (2018).
35. X. Vidal and J. Martorell, "Generation of light in media with a random distribution of nonlinear domains," *Phys. Rev. Lett.* **97**, 013902 (2006).
36. X. Chen and R. Gaume, "Non-stoichiometric grain-growth in ZnSe ceramics for $\chi^{(2)}$ interaction," *Opt. Mater. Express* **9**, 400–409 (2019).
37. R. Savo et al., "Broadband Mie driven random quasi-phase-matching," *Nat. Photon.* **14**, 740–747 (2020).
38. B. Jeon, J. S. Yoo, and J. D. Lee, "Electrophoretic deposition of ZnO:Zn phosphor for field emission display applications," *J. Electrochem. Soc.* **143**, 3923 (1996).
39. Z. Zhou et al., "Far-field super-resolution imaging by nonlinearly excited evanescent waves," *Adv. Photon.* **3**(2), 025001 (2021).
40. G. Yi et al., "Nonlinear third harmonic generation at crystalline sapphires," *Opt. Express* **25**, 26002–26010 (2017).

Zhihao Zhou received his BS degree from the Department of Physics at East China Normal University in 2017, and graduated from Shanghai Jiao Tong University in 2022, where he got his PhD. He recently started his career in industry.

Wenjie Wan received his BE degree from the Hong Kong University of Science and Technology and his PhD from Princeton University in 2010. After a year of postdoctoral training at Yale University, he joined the faculty of Shanghai Jiao Tong University in 2011, where he is currently an associate professor. His current research interests include nonlinear optics, nanophotonics, and optical microcavity.

Biographies of the other authors are not available.